ITER Performance Study with the Presence of Internal Transport Barrier

Thawatchai Onjun

Plasma and Fusion Research Unit, Sirindhorn International Institute of Technology, Thammasat University, Pathum Thani, Thailand

(Received: 5 September 2008 / Accepted: 11 April 2009)

Self-consistent modeling of the International Thermonuclear Experimental Reactor (ITER) has been carried out using the 1.5D BALDUR integrated predictive modeling code. In these simulations, the boundary is taken to be at the top of the pedestal, where the pedestal values are described using a theoretical-based pedestal model. This pedestal temperature model is based on magnetic and flow shear stabilization width scaling and ballooning mode pressure gradient model. The pedestal temperature model is used together with a Mixed B/gB core transport model, which can include the ITB effect. It is found that the formation of an ITB has a strong impact on both temperature profiles, especially near the center of the plasma. With the ITB effect is included, the central ion temperature increases significantly. The increase of central temperature results in a significant improvement of alpha power production and, consequently, fusion performance. It is observed that in most of the plasma core, the ion thermal diffusivity is smaller with an ITB included than in those without the ITB in the ITER simulations. This reduction in the diffusivity results in stronger gradients and, consequently, higher values of the central temperature.

Keywords: Plasma, Fusion, ITER, ITB, ETB, Pedestal

1. Introduction

The International Thermonuclear Experimental Reactor (ITER) is an international collaborative effort with an aim to demonstrate the scientific and technological feasibility of nuclear fusion using the magnetic confinement fusion concept [1]. The goal of ITER is to produce plasmas with a sufficiently high energy density for a long enough time to achieve sustained high-performance fusion burning. Producing fusion reactions which satisfy such a condition inside a tokamak requires the ability to both heat and contain high-temperature plasmas. Due to the fact that high confinement mode (*H*-mode) discharges in tokamaks generally provide excellent energy confinement and have acceptable particle transport rates for impurity control, many fusion experiments such as ITER are designed to operate in the *H*-mode regime. The improved performance of *H*-mode mainly results from the formation of the edge transport barrier (ETB) [2], called the pedestal. It is also known that performance of *H*-mode plasma can be further improved with the presence of a transport barrier inside plasma, called the internal transport barrier (ITB) [3]. The presence of ITB in *H*-mode plasma results a complicated scenario and yields an improve performance of that plasma.

The projections of ITER have been carried out in many scenarios using various integrated modeling codes [4-8]. For example, the BALDUR integrated predictive modeling code [9] was used to predict the performance of ITER for the standard *H*-mode scenario [4, 6-8]. The performance of ITER was evaluated in term of fusion *Q*. Note that fusion *Q* is the ratio of a fusion power with an applied heating power. A range of the performance is predicted. It was found that the predicted performance of ITER using BALDUR code with the Mixed Bohm/gyroBohm (Mixed B/gB) transport code is relatively low compared to those using other transport codes [6-8]. It is worth noting that Mixed B/gB was developed using the JET plasma. In those previous works [6-8], the effect of ITB was not included in the simulations. As a result, it is interesting to explore the *H*-mode scenario of ITER when ITB is present.

In this work, the preliminary study of the ITER in the *H*-mode scenario with the presence of ITB is carried out. The *H*-mode is represented by the formation of ETB. The ETB is described by a pedestal model based on magnetic and flow shear stabilization, and ballooning mode instability. For the ITB, the ITB is formed by the suppression of core anomalous transport. This paper is organized as follows: brief descriptions for a BALDUR integrated predictive modeling code, anomalous transport models, and pedestal models are given in section 2. The ITER prediction using a BALDUR integrated predictive modeling code is described in section 3, while conclusion is given in section 4.

2. BALDUR Code

The BALDUR integrated predictive modeling code is used to compute the time evolution of plasma profiles including electron and ion temperatures, deuterium and tritium densities, helium and impurity densities, magnetic *q*, neutrals, and fast ions. These time-evolving profiles are computed in the BALDUR integrated predictive modeling code by combining the effects of many physical processes self-consistently, including the effects of transport, plasma

author's e-mail:thawatchai@siit.tu.ac.th

heating, particle influx, boundary conditions, the plasma equilibrium shape, and sawtooth oscillations. Fusion heating and helium ash accumulation are also computed self-consistently. The BALDUR simulations have been intensively compared against various plasma experiments, which yield an over all agreement within 10% relative RMS deviation [10, 11]. In BALDUR code, fusion heating power is determined by the nuclear reaction rates and a Fokker Planck package to compute the slowing down spectrum of fast alpha particles on each flux surface in the plasma. The fusion heating component of the BALDUR code also computes the rate of the production of thermal helium ions and the rate of the depletion of deuterium and tritium ions within the plasma core. The effect of sawtooth oscillation is also included, where a Porcelli sawtooth model [12] is used to determine a sawtooth crash and a modified Kadomtsev magnetic reconnection model [13] is used to describe the effects of sawtooth crash.

2.1 ITB model

In this work, the ITB is formed by the suppression of core anomalous transport due to ω_{ExB} flow shear and magnetic shear. This effect is included in the anomalous core transport called "the Mixed Bohm/gyroBohm (Mixed B/gB) model [14]. This core transport model is an empirical model. It was originally a local transport model with Bohm scaling. A transport model is said to have "Bohm" scaling when the transport diffusivities are proportional to the gyro-radius times thermal velocity over a plasma linear dimension such as major radius. Transport diffusivities in models with Bohm scaling are also functions of the profile shapes (characterized by normalized gradients) and other plasma parameters such as magnetic q, which are all assumed to be held fixed in systematic scans in which only the gyro-radius is changed relative to plasma dimensions. The original JET model was subsequently extended to describe ion transport, and a gyroBohm term was added in order for simulations to be able to match data from smaller tokamaks as well as data from larger machines. A transport model is said to have "gyroBohm" scaling when the transport diffusivities are proportional to the square of the gyroradius times thermal velocity over the square of the plasma linear dimension. The Bohm contribution to the JET model usually dominates over most of the plasma. The gyroBohm contribution usually makes its largest contribution in the deep core of the plasma and plays a significant role only in smaller tokamaks with relatively low power and low magnetic field. To include the ITB effect, the Bohm contribution is modified. The Bohm/gyroBohm transport model with ITB effect included [15] can be written in the following way:

$$\chi_e = 1.0\chi_{gB} + 2.0\chi_B \quad (1)$$

$$\chi_i = 0.5\chi_{gB} + 4.0\chi_B + \chi_{neo} \quad (2)$$

$$D_H = D_Z = \left[0.3 + 0.7\rho\right]\frac{\chi_e\chi_i}{\chi_e + \chi_i} \quad (3)$$

where

$$\chi_{gB} = 5\times10^{-6}\sqrt{T_e}\left|\frac{\nabla T_e}{B_\phi^2}\right| \quad (4)$$

$$\chi_B = 4\times10^{-5}R\left|\frac{\nabla\left(n_eT_e\right)}{n_eB_\phi}\right|q^2\left(\frac{T_{e,0.8}-T_{e,1.0}}{T_{e,1.0}}\right)$$

$$\Theta\left(-0.14+s-\frac{1.47\omega_{E\times B}}{\gamma_{ITG}}\right) . \quad (5)$$

The ω_{ExB} is the flow shearing rate and the value of γ_{ITG}, the ITG growth rate, is estimated as v_{ti}/qR, in which v_{ti} is the ion thermal velocity. In, BALDUR code, the ω_{ExB} shearing rate is calculated as follows:

$$\omega_{ExB} = \left|\frac{RB_\theta^2}{B_T}\frac{\partial\left(E_r/RB_\theta\right)}{\partial\psi}\right|, \quad (6)$$

where R is the major radius, B_θ and B_T are the poloidal and toroidal magnetic fields, respectively, Ψ is the poloidal flux, and E_r is the radial electric field for the main plasma ions, which is calculated as follows:

$$E_r = \frac{1}{Zen_i}\frac{\partial p_i}{\partial r} - v_\theta B_T + vB_\theta, \quad (7)$$

where $\partial p/\partial r$ is the pressure gradient, v_θ and v are the poloidal and toroidal velocities and, n_i is the ion density, Z is the ion charge number and e the elementary charge. Note that in this work, the toroidal velocity is taken directly from experiment.

2.2 ETB models

In the BALDUR code, a boundary condition is set at the top of the pedestal. As a result, the code requires both temperature and density at the top of the pedestal. A simple model for estimating pedestal temperature can be developed by using the values of pedestal width and pedestal pressure gradient [16]. In this work, the pedestal width is estimated using a magnetic and flow shear stabilization concept ($\Delta = C_w\rho s^2$) [17] and the pedestal gradient is estimated using first ballooning mode pressure gradient limit. The effect of bootstrap current and geometry are also considered. The pedestal temperature takes the following form:

$$T_{ped}\left(keV\right) = 0.323C_W^2\left(\frac{B_T}{q^2}\right)^2\left(\frac{M_i}{R^2}\right)\left(\frac{\alpha_c}{n_{ped,19}}\right)^2 s^4, \quad (8)$$

where $n_{ped,19}$ is the electron density at the top of the pedestal in units of 10^{19} m^{-3}.

In general, the pedestal density (n_{ped}) in *H*-mode plasmas is a large fraction of line average density (n_l). In the report by G. Bateman *et al*. [4], the pedestal density is taken to be

$$n_{ped} = 0.71\, n_l . \qquad (9)$$

3. Simulations of ITER

The BALDUR integrated predictive transport modeling code is used to carry out the simulations of ITER with the designed parameters (R = 6.2 m, a = 2.0 m, I_p = 15 MA, B_T = 5.3 T, κ_{95} = 1.70, δ_{95} = 0.33 and n_l = 1.0x10^{20} m^{-3}). In this work, the plasma current and density are gradually ramped up to the target values within 100 sec. The plasma current at the start up phase is 3 MA and is slowly increased to the target. It is found that the plasma reaches the *H*-mode phase at the time of 2 sec. It is worth noting that there are several physics that have not been included in these simulations, such as ELM crashes and neoclassical tearing modes. As a result, the simulation results are not appropriate to represent the dynamic of plasma in ITER. However, these simulations include enough physics to describe plasma when it reaches the steady state. The simulations still yield complex and interesting interactions within the plasma itself — such as the self plasma heating by the alpha particle and redistribution of heating power after sawtooth crash — still occurs and leads to interesting observation. Note that the sawtooth oscillation is considered during the time of 10 sec to 995 sec. For each simulation, an anomalous transport is calculated using the Mixed B/gB transport model, while the neoclassical transport is computed using the NCLASS module [18]. The boundary conditions are provided at the top of the pedestal by the pedestal model described above, which will be varied later to observe its sensitivity. It is assumed that the electron and ion pedestal temperatures are of the same values. In these simulations, the auxiliary heating power of 40 MW, which is a combination of 33 MW NBI heating power with 7 MW of RF heating power, is used.

A slow current ramp (reaching the target value in 100 sec) is used during the first stage of each simulation of the burning plasma experiments. The plasma density is also ramped up to the final plasma density during this stage; while the full heating is applied since the beginning. Note that the plasma density is ramping up and controlled at the target values by using gas puffing method. During this ramp, the plasma makes a transition from *L*-mode to *H*-mode. Since there is a strong heating at the beginning, all simulations enter the *H*-mode phase approximately within 2 sec. In figure 1, the toroidal velocity and ω_{ExB} used in this work are shown. The toroidal velocity is taken from an optimized magnetic shear (OS) discharge in JET experiment, discharge 40542. The ω_{ExB} profile is calculated by Eqs. (6) and (7) by using the toroidal velocity from the top panel of figure 1.

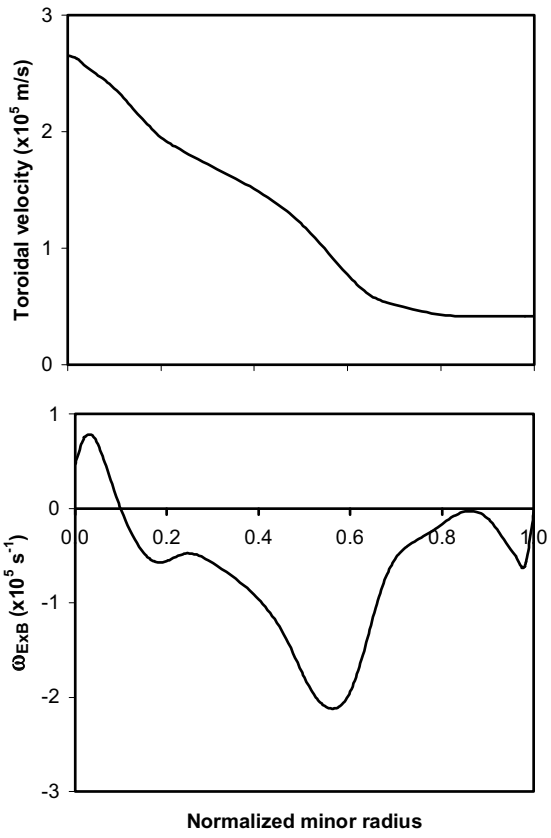

Fig.1 The toroidal velocity (top) and ω_{ExB} (bottom) profiles used in this work are plotted as a function of a normalized minor radius. Toroidal velocity profile is taken from JET experiment (discharge 40542), while the ω_{ExB} is calculated using Eqs. 6 and 7.

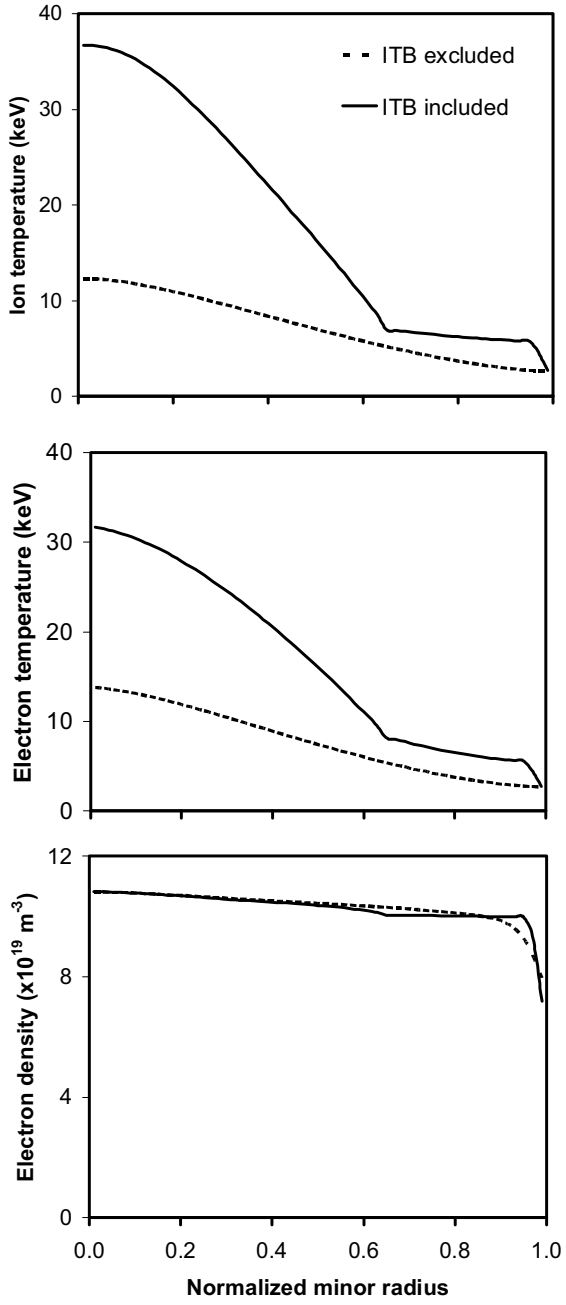

Fig.2 The profiles for ion (top) and electron (middle) temperatures and electron density (bottom) are plotted as a function of a normalized minor radius at time of 1000 sec. The simulations are carried out with and without the effect of ITB.

Figure 2 shows profiles for ion temperature (top), electron temperature (middle) and electron density (bottom) as a function of normalized minor radius at a time of 1000 sec. The simulations are carried out using Mixed B/gB model with the effects of ITB excluded and included. It can be seen that all ion and electron temperature profiles are peak. When the effects of ITB are included, the central temperature increases significantly, where the edge remains the same. It is found that the pedestal is almost constant after the density reaches a target value. It is worth noting that the ion pedestal temperature is assumed to be the same with the electron temperature. Also, the effect of ELMs is not included in these simulations. For the electron density, the profile shape is a relatively small peak. It is also found that in both simulations, the electron density profile is almost the same, which means that the formation of ITB does not have an impact of density profile. In addition, it is found that the ITB effective region is up to $\rho = 0.6$. This ITB region results from the reduction of the transport in the region close to the plasma core, which can be seen in figure 3. It is worth mentioning that the safety factor profile in this ITER simulation is a monotonic profile with a flat profile near the plasma center, which is different from what observed in JET discharge 40542. This subject is beyond the scope this paper. It rather leaves this issue for future work.

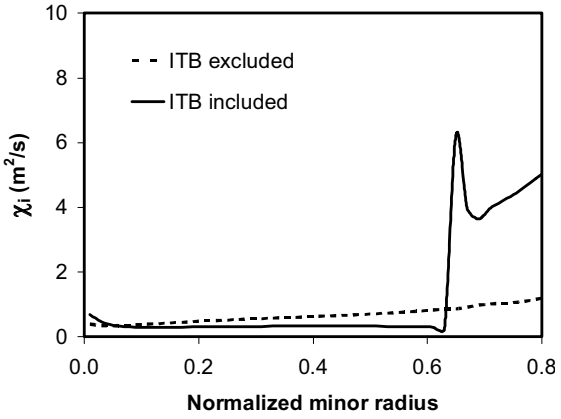

Fig. 3 The profile of total ion diffusivity is plotted as a function of normalized minor radius from the center up to a normalized radius of 0.8 at time of 1000 sec. The simulations are carried out with and without ITB effects.

The summary of central temperature and density is shown in Table 1. It can be seen that the central ion temperature increases significantly when the ITB effects are included. The central ion temperature in the simulation when ITB is included is about 36.7 keV, which is in effective range for fusion production. The central ion and electron temperatures increase 198% and 130%, respectively. This increase of central temperature will have a strong impact on the plasma stored energy and the nuclear fusion power production.

Figure 4 shows the plasma stored energy as a function of time between 900 sec to 1000 sec. It can be seen that the value of plasma stored energy is in the range

of 200 MJ for the simulation with ITB excluded; while the plasma stored energy increases to 450 MJ when ITB is included.

Table 1: The summary of central temperature and density at the time of 1000 sec.

Parameters	ITB excluded	ITB included
$T_{i,0}$ [keV]	12.3	36.7
$T_{e,0}$ [keV]	13.8	31.7
$n_{e,0}$ [10^{19} m^{-3}]	10.8	10.8
T_{ped} [keV]	2.6	2.6
$n_{e,ped}$ [10^{19} m^{-3}]	7.1	7.1

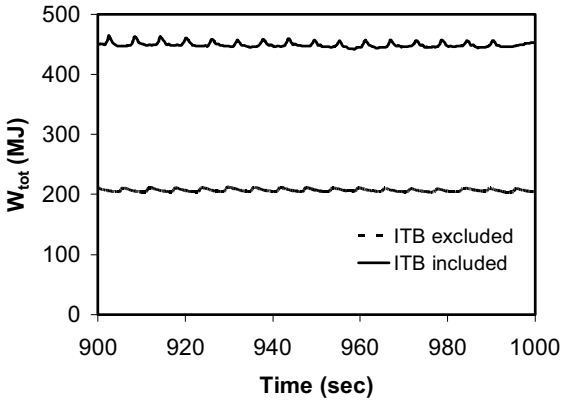

Fig.4 The plasma stored energy is plotted as a function of time for the simulation when ITB is excluded and included.

There are two types of auxiliary heating used in the ITER simulation. The total amount of neutral beam injection heating power, P_{NBI}, is 33 MW. Another source of auxiliary heating is the RF heating. The total amount of RF heating power is 7 MW. For simplicity, the RF heating profiles are taken to be a parabolic shape, although it is recognized that the physics of RF heating might be more complicated in the ITER plasma. Note that Ohmic heating is small compared to other types of heating. The alpha heating power is also shown in figure 5. It is found that the alpha heating power is the main heating source of the plasma in the simulation with ITB. However, the alpha power heating is slightly higher than the NBI heating power in the simulation without ITB.

Figure 6 shows the alpha power production from the simulations when ITB is excluded and included. It can be seen that the alpha power from the simulation when ITB is included is much higher than that without ITB. The average of alpha power during the time of 900 sec to 1000 sec is summarized in Table 2. The fusion performance can be evaluated in term of Fusion Q, which can be calculated as

$$\text{Fusion } Q = \frac{5 \times P_{\alpha,avg}}{P_{AUX}},$$

where $P_{\alpha,avg}$ is an average alpha power and P_{AUX} is an auxiliary heating power (equal to 40 MW for these simulations). It can be seen in Table 2 that the Fusion Q increases by 200% when ITB is included.

Table 2: The summary of average alpha power and corresponding fusion Q.

Parameters	ITB excluded	ITB included
P_{α} [MW]	26.3	124.9
Fusion Q	3.3	15.6

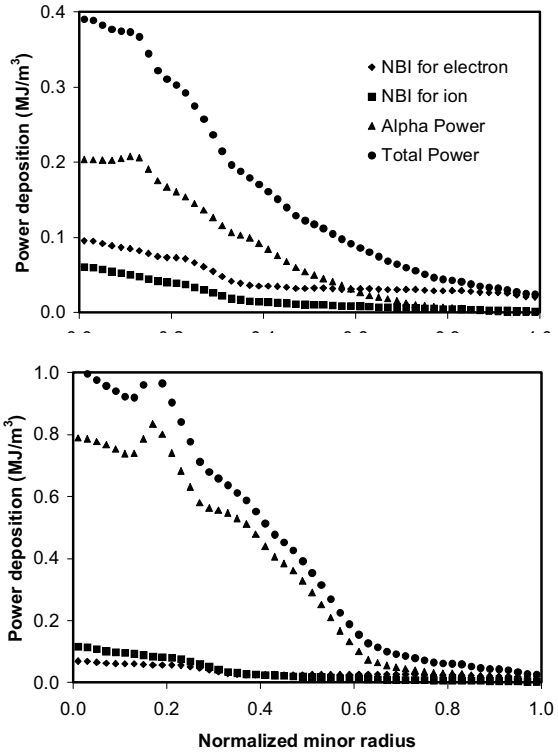

Fig.5 The power deposition profiles are shown as a function of normalized minor radius for the simulations when ITB is excluded (top) and included (bottom).

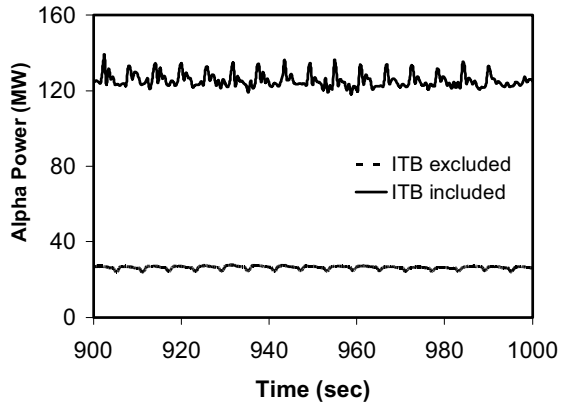

Fig.6 The alpha plasma production is plotted as a function of time for the simulation when ITB is excluded and included.

4. Conclusion

Self-consistent simulations of ITER have been carried out using BALDUR code, where the effects of both ETB and ITB are considered. The ETB condition is provided by the pedestal model based on magnetic and flow shear stabilization width scaling together with ballooning mode instability pressure gradient model; while the formation of ITB results from the suppression of transport by E_rxB shear and magnetic shear. It is found that the formation of an ITB has a strong impact on both temperature profiles, especially near the center of the plasma. Because of the inclusion of the ITB effect, the central ion temperature increases more than a factor of two. The increase of central temperature results in a significant improvement of alpha power production and, consequently, fusion performance. In the simulation with ITB, it is observed the reduction of ion thermal transport in most of the plasma core, which results in stronger gradients and, consequently, higher values of the central temperature.

5. Acknowledgments

The author thanks Prof.Dr.A H Kritz, Dr.G Bateman, Dr.V Parail, Dr.A Pankin, Dr.S Suwanna, Dr.N Poolyarat, and Dr.R Picha for their helpful discussions and supports. This work is supported by Commission on Higher Education (CHE) and the Thailand Research Fund (TRF) under Contract No. RMU5180017.

6. References

[1] R. Aymar *et al.*, Plasma Phys. Control. Fusion **44**, 519 (2002)
[2] A. Hubbard, Plasma Phys. Control. Fusion **42**, A15 (2000)
[3] J.W. Connor *et al.,* Nucl. Fusion **44**, R1 (2004)
[4] G. Bateman *et al.*, Plasma Phys. Control. Fusion **45,** 1939 (2003)
[5] T. Onjun *et al.*, Phys. Plasmas **12**, 082513 (2005)
[6] T. Onjun *et al.*, J. of Physics: Conference Series **123**, 012034 (2008)
[7] K. Tharasrisuthi et al., Thammasat International Journal of Science and Technology **13**, 45 (2008)
[8] R. Picha *et al.*, Proc. of 35th EPS Conference on Plasma Physics, Hersonissos 9-13 June 2008 (2008)
[9] C. E. Singer *et al.*, Comput. Phys. Commun. **49,** 399 (1988)
[10] D. Hannum *et al.*, Phys. Plasmas **8,** 964 (2001)
[11] T. Onjun *et al.*, Phys. Plasmas **8**, 975 (2001)
[12] F. Porcelli *et al.*, Plasma Phys. Control. Fusion **38**, 2163 (1996)
[13] G. Bateman *et al.*, Phys. Plasmas **13,** 072505 (2006)
[14] M. Erba *et al.*, Plasma Phys. Control. Fusion **39,** 261 (1997)
[15] T. J. J. Tala, *et al*., Phys. Control. Fusion **43**, 507 (2001)
[16] T. Onjun *et al.*, Phys. Plasmas **9**, 5018 (2002)
[17] M. Sugihara *et al.,* Nucl. Fusion **40**, 1743 (2000)
[18] W. A. Houlberg *et al.*, Phys. Plasmas **4**, 3231 (1997)